Fractal sandstone pores: Automated measurements using scanning-electron-microscope images

C. E. Krohn and A. H. Thompson
Exxon Production Research Company, P.O. Box 2189, Houston, Texas 77001
(Received 25 November 1985)

An automatic technique has been developed to measure precisely the fractal dimension of the microstructure of sandstones from scanning-electron-microscope (SEM) images of fracture surfaces. The technique involves digitizing the images, filtering, counting geometrical features as a function of feature size, and fitting feature histograms. The magnification of the SEM is changed to cover 2.5 orders of magnitude in feature sizes. A power-law model, which includes the resolution of the digital filter, accounts for the feature size distributions for all magnifications and the scaling from magnification to magnification. Results have been obtained for a dozen sandstones, and the fractal dimension is observed to range from 2.55 to 2.85. The precision for averaged images is ±0.01. In addition, a long-length limit to the fractal regime is defined and measured.

I. INTRODUCTION

Katz and Thompson[1] have proposed that the pore spaces of sandstones are fractals, and they presented several measurements to support their proposal. These included manual feature-counting measurements on scanning-electron-microscope (SEM) images and autocorrelation measurements on thin sections. They developed a nucleation and growth model of diagenesis, the rock-formation processes occurring after deposition, which could account for fractal pore spaces with different fractal dimensions for different sandstones. In addition, they discussed implications for the sandstone porosity and transport properties.

We have developed an automated technique for making SEM measurements, and a large body of data has been obtained for sandstones that confirms the fractal nature of many of the pore spaces. The technique allows the determination of the fractal dimension with high precision, and the values agree with other methods. In addition to the fractal dimensions which vary from sample to sample, the long-length limit to the fractal regime has been measured. The effect of varying and averaging positions on the sample as well as other aspects of the technique have been investigated.

Fractal properties are often determined by measuring the length of an interface as a function of the unit of measure.[2] Unfortunately, the SEM intensity for a fracture surface is not directly correlated to the surface profile, and a length along the surface is not easily measured. In addition, the intensity changes with particle size and position as well as with magnification. Any method which explicitly uses the intensity of the SEM beam, for example, a power-spectrum measurement, is suspect. Serra[3] used the autocovariance to measure the fractal dimension of clay rocks assuming the same behavior of relative intensity for large and small particles at all magnifications. This assumption is not generally valid. To avoid this problem, we developed a statistical counting method which does not depend directly on the SEM intensity.

We determine the number of structural features found at the interface between rock space and pore space and compare that number to the feature size. The edge of a feature is defined to be a change in contrast in the secondary-electron intensity of the SEM which results in a local maximum in intensity. Typically, edges appear bright on SEM images. Features represent grains or clay particles as well as pits and bumps along the surfaces of grains and clay particles. The feature size is the distance between adjacent maxima. An analysis based on the counting of features will indicate if features of a particular size dominate the pore geometry, or if there is an absence of features of a particular size.

The method chosen here for measuring the fractal dimension reflects the physics of interest. We are interested in the transport properties of fluids in the pore space. The influence of the pore wall can be characterized by determining the number and size of geometric features that protrude into the pore space and scatter ions or fluid elements in the pore space. We envision the structure on a fracture surface of a porous rock to be primarily associated with the pore-rock interface. This will be particularly true for fine structure smaller than the size of a grain lying below the fracture surface. Reference 1 supports this assumption by showing that the measured fractal parameters correctly predict trends in porosity.

Katz and Thompson[1] treat a single horizontal scan of the SEM beam as a line intersecting the rock-pore interface. For fractal behavior, the number of features counted per centimeter $N(l)/\mathrm{cm}$ for features of size l can be expressed as

$$N(l)/\mathrm{cm} \propto l^{2-D}, \tag{1}$$

where D is the fractal dimension and l includes all feature sizes from l_1 to l_2. The limits for fractal behavior l_1 and l_2 are expected to extend from around 10 Å to 100 μm in a typical sandstone. Beyond the long-length limit l_2, the sample appears homogeneous, and the exponent in Eq. (1) relating the number of features to the feature size should be equal to -1. In this regime, the geometrical features appear as statistically random noise.

In the rest of this paper, the technique and results will be described and discussed. The description of the technique includes the feature-counting method, a derivation of the model feature distribution, and the fitting procedure. The technique will be evaluated including a comparison of the automatic technique and other methods, the effect of varying and averaging position on the sample, and the effect of noise and filtering on the results. Finally, data from a number of sandstones are presented, and the confidence in the observed results is evaluated.

II. TECHNIQUE

The technique includes image digitization, filtering, counting features, and fitting the resulting feature histogram. In this section, the feature-counting method, the model feature distribution, and the fitting procedure are described.

A. Image digitization

The signal-to-noise ratio and the geometrical accuracy of the image digitization are important for a feature-counting technique. Most commercial SEM digitization systems either involve operating the beam at TV scan rates with a very poor signal-to-noise ratio, or rely on TV camera digitization of photographs which have very poor geometrical accuracy.[4] To overcome these limitations, we built a SEM digitization system based on the Hewlett Packard 9836C computer. Images were digitized in the photo mode of the SEM; 512 points were digitized per line, and 512 lines were digitized per image with a 12-bit analog-to-digital (A/D) converter. The geometrical accuracy and the signal-to-noise ratio of the images were limited by the JEOL 35C SEM and not by the digitization system. The geometrical accuracy was better than 0.09%, and the signal-to-noise ratio was better than -47 dB. A number of images could be quickly digitized, displayed on the cathode ray tube (CRT), and transferred to magnetic tape or Winchester disc.

Before digitizing an image, a position was selected on the fracture surface. This position could have been chosen at random if many locations were being digitized. Instead, a highly structured area was selected because it was not feasible to collect such a large amount of data. In particular, a position was chosen where the structure persisted to the highest magnifications. To obtain the best signal-to-noise ratio, areas were chosen with minimal relief or the smallest change in average intensity for different sections of the image. At each location, 18–20 different magnifications were digitized. Each digitized image was stored on a Winchester disc and output to magnetic tape. In the analysis, the images could be examined, and areas could be eliminated from feature counting if they were off the edge of the sample or were out of focus.

B. Filtering

A digital low-pass filter was convolved with the data in order to establish a resolution which was uniform at all magnifications and independent of the optics of the SEM. This filter must be both transient free and linear phase. A transient-free filter is one which does not have an oscillating impulse response function; its response to a square wave should be smooth without any overshoots. Such overshoots added to the SEM signal would be counted as extra features. Linear phase is required so that the time shift for each feature does not vary for different frequencies resulting in erroneous feature size measurements.

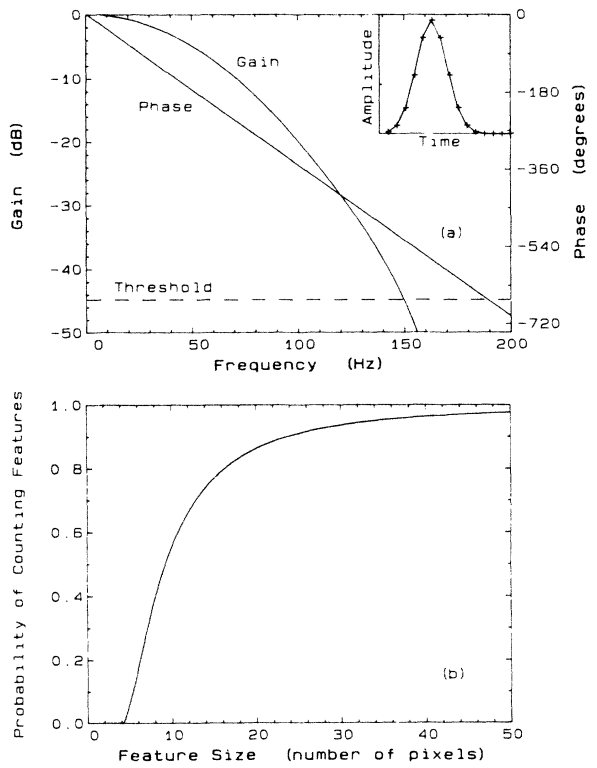

FIG. 1. Digital filter characteristics. (a) Frequency response showing cutoff by amplitude threshold. Impulse response is in inset. (b) Probability of resolving a feature as a function of the feature size.

A finite-impulse-response (FIR) filter was designed with a Gaussian impulse response which was truncated by setting anything less than 0.5% of the Gaussian peak equal to zero as shown in the inset of Fig. 1(a). Typically, the Gaussian half-width was set equal to 1.75. With this value, the filter had 11 nonzero values. One hundred lines of the image were convolved with the filter and the derivative of the filter to produce the filtered data and the filtered derivative.

C. Counting features

Local maxima were defined to be feature edges. In counting the features, care was taken not to count features which corresponded to noise by setting an amplitude threshold for the counting of features. The procedure for counting features without counting noise was as follows: The first pair of neighboring maxima and minima which had a difference in intensity above the threshold was found; then, the next pair was found; the distance between

the two maxima was measured, and any pairs between were ignored. In addition, the total dead space in the image was computed so that the number of features could be normalized by the area measured. Dead space corresponded to space between the first or last maximum in a line and the edge of the image. In addition, the option existed to exclude poor data areas from the image.

Setting an amplitude threshold to distinguish between signal and noise establishes a cutoff for the resolution. Figure 1(a) is a graph of the filter response. The amplitude cutoff sets a limit to the high frequencies which are counted. However, the threshold needs to be set as a fraction of the signal size at each magnification to ensure a constant frequency cutoff. The signal size was measured by counting the features using a constant threshold, and measuring the average amplitude difference between neighboring minima and maxima for features of a size less than the cutoff of the filter. Typically, the amplitude was measured for features of size between $\frac{15}{512}$ and $\frac{20}{512}$ of the field of view. The threshold for the magnification with the lowest value of the averaged amplitudes was set at a voltage which was higher than measured noise from the SEM such as 0.03 V (−44 dB for a 5-V signal). Then, the thresholds for the other magnifications were set proportionally to their averaged amplitudes, and the count was repeated.

The result of the counting procedure for a number of repetitive lines is a histogram of the number of features of each feature size. A small bin size was used in computing the histogram by interpolating between pixels for the locations of zero crossings and measuring feature sizes to one-tenth of a pixel. Figure 2 illustrates the procedure for counting features. Panel (a) of the figure is a plot of the intensity of the SEM beam for a single scan. Panel (b) shows the filtered intensity, and the locations of all feature edges which were counted. The counting of features for a hundred such lines yields a feature histogram which is shown in panel (c) of the figure.

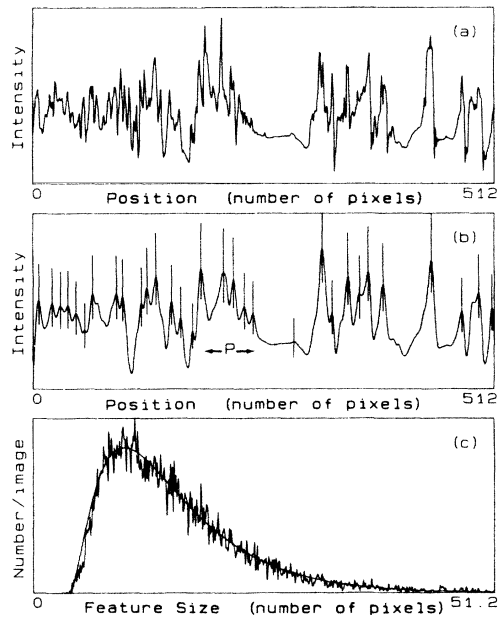

FIG. 2. Illustration of feature counting. (a) Digitized SEM data for a single horizontal line. (b) Same data filtered with edges of counted features marked by vertical lines. (c) Histogram for 100 lines with fit of histogram using Eq. (6). "P" marks a feature in scan (b) which is not counted at this magnification.

D. Model feature distribution

In this section, the model feature distribution will be derived based on a power-law relationship between the number of features per unit length and the feature size, Eq. (1). Since the measurements were made from images, a convenient measure of the feature size is in terms of pixels, where a pixel is $\frac{1}{512}$ of the image. The digitized data are represented by a sequence of intensities $I(J)$, where J is a pixel ranging from 1 to 512. The feature size L for a feature with an edge at J_1 and at J_2 is J_2-J_1. The width in centimeters of the field of view for each image is 12 divided by the magnification or $12/M$. Thus the number of features per centimeter from Eq. (1) becomes

$$N(L)/\mathrm{cm}=A\,(12L/512M)^{2-D}\,, \tag{2}$$

where L is the feature size in pixels, A is a proportionality constant, and M is the magnification.

The number of features actually counted $N(L)$ in the feature histogram is equal to the number of features per centimeter times the probability of detecting a feature times the distance in centimeters over which the features are counted. We write,

$$N(L)=N(L)/\mathrm{cm}P(L)R(L)\ (\mathrm{cm})\,. \tag{3}$$

The probability $P(L)$ of detecting a feature of size L is set by the digital filter, and it can be determined explicitly by performing the Fourier transform of the impulse response and expressing the amplitude as a function of distance rather than frequency. The Fourier transform of the Gaussian filter is also a Gaussian in the frequency domain, and the gain is 1.0 at zero frequency. The probability of resolving a feature is directly dependent on the amplitude of the filter, with the probability equal to 1.0 at the largest feature sizes. To simulate the amplitude threshold for the removal of noise, we set the probability to zero for L less than the value L_0 where the amplitude of the filter becomes less than the signal-to-noise threshold for the detection of features. The value L_0 is the same for all magnifications and was typically around $\frac{42}{5120}$ of the field of view. This expression works well in describing the resolution of the counted features, but it was more plausible to smooth the transition at L_0 by using a Gaussian probability of detecting the features slightly above L_0. This filter function is shown in Fig. 1(b).

The distance $R(L)$ available for counting features of size L is the product of the width of the field of view times the fraction of that field of view which is unoccupied by smaller features, i.e., large features are not seen if small features on top of them are resolved. For example, in Fig. 2(b) the particle marked as P will not be counted as a feature at this magnification because smaller features sitting on top of P are resolved. P will be counted at a lower magnification. Thus $R(L)$ can be expressed as a

function of the number of features counted for sizes less than L. The fraction of the field of view $F(L-1)$ occupied by features of size less than L is

$$F(L-1)=\frac{1}{512}\sum_{K=0}^{K=L-1} KN(K)\ , \tag{4}$$

where K is a feature size smaller than L. The function $F(L)$ will be called the cumulative feature distribution in this paper. As L gets large, $F(L)$ must become equal to 1.0. Since $R(L)$ is the width of the field of view in centimeters times the fraction of the field of view unoccupied by smaller features, then

$$R(L)=[(12\text{ cm})/M][1-F(L-1)]\ . \tag{5}$$

Substituting for $N(L)$/cm in Eq. (3), an expression for the feature histogram is obtained:

$$N(L)=A(12L/512M)^{2-D}P(L)(12/M)[1-F(L-1)]\ , \tag{6}$$

where $F(L-1)$ is given by Eq. (4). This expression has only two unknown parameters, A and D. The feedback term $[1-F(L-1)]$ ensures that $F(L)$ equals 1.0 at large L. In other words, as larger and larger features are counted, the field of view eventually fills up, and fewer features are counted. In addition, this expression shows that at low magnifications where many small features are detected in each image, few large features are detected. At higher magnifications where fewer small features are detected in each image, more large features are detected. Also, it can be seen that it is not possible to divide out the parameter A because of the feedback. Thus A and D must be determined together. Figure 2(c) includes a fit of Eq. (6) to the measured histogram.

E. Log-log plots of the feature histograms

The measured feature histograms for each magnification can be placed on a log-log plot using Eq. (3). The number of features per unit length is obtained by dividing the histograms by $P(L)$, the probability of detecting a feature, and by $R(L)$, the measuring distance. $R(L)$, which is defined in Eq. (5), is determined from the measured cumulative feature distributions. A linear least-squares fit to the results demonstrates power-law behavior and gives good starting parameters for fits of the histograms themselves.

F. Fitting the feature histograms

Equation (6) was used to fit the measured histograms. The object of the fitting routine was to determine if the measured feature distribution could be described by a power law over a certain range of lengths, and to determine the fractal dimension. Fits of a model to the feature histograms have several advantages over a linear least-squares fit to linearized data as described above. When the data are linearized, the errors for each magnification are inappropriately weighted in determining the parameters.[5] In particular, computing the logarithm generates a larger error for the higher magnifications than for the lower magnifications; thus, the fit will depend inappropriately on the values from the higher magnifications. In addition, the fits to the feature histograms have the advantage that the parameters are adjusted to match the shape of the curve and having too many or too few counts at one feature size will not change the value of the fitted parameters as much as it would if all the points were linearized.

The fitting routine was done iteratively. An initial range of magnifications was selected from log-log plots of the data, and a single fit was done simultaneously to the feature histograms for all the magnifications in that range using single values of A and D. After performing the fit, the residues (sum of the measured values minus fitted values) for each magnification were examined. If low magnifications which were not in the fractal regime were included in the fit, the residues became systematically negative. Performing repeated fits and checking the residues allowed the range of fractal behavior to be determined precisely. Once the range was determined, tests of the errors in the fitted parameters were made by checking the variation in the parameters as magnifications were removed from the range included in the fit.

The best fit was selected by minimizing the weighted sum over all the magnifications of the sum of the errors squared. The magnifications were weighted so that the magnifications with the better statistics had a greater input into the fit. The weights were equal to the square root of the total number of features counted at that magnification divided by the square root of the total number of features in the magnification range. The sum of the errors squared for each magnification was limited to the feature sizes which were larger than two times L_0, the length at which the probability of detecting a feature became larger than zero, and less than the length where the histogram value decreased to 10% of the maximum.

In order to observe the scatter in the data from magnification to magnification, individual fits were also done for each magnification. The number of features $N(L)$/cm for a point L near the peak of the fitted histogram was selected as representative of that magnification and plotted on a log-log plot. The points representing each magnification were then compared to the results obtained from the simultaneous fit to all the magnifications. Beyond the fractal regime, a line of slope -1 was fitted to the points representing each magnification.

The results of the fitting procedure included evaluating whether or not there was power-law behavior, determining if there was a limit to the power-law regime, and measuring that limit. The error in the fractal-dimension measurement was also estimated. Additional positions could be naturally included in the analysis by averaging the feature distributions for each magnification.

III. RESULTS

A. Fits of the feature histogram

Figure 2(c) demonstrates how well the model feature distribution fits the measured one. The model, which uses only two adjustable parameters, is able to match the histo-

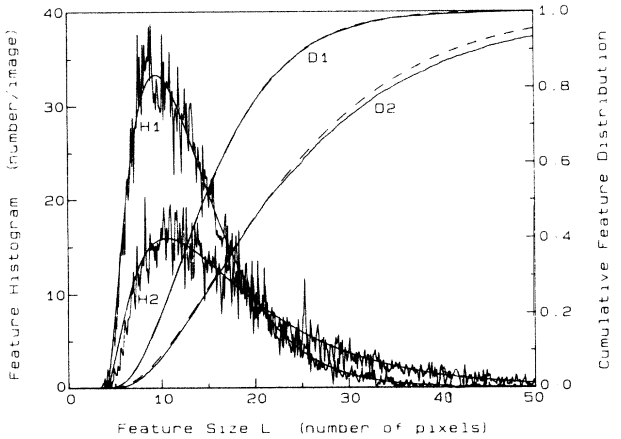

FIG. 3. Feature histograms for a low (H1) and high magnification (H2) showing fits to Eq. (6). Also shown are the cumulative feature distributions (D1,D2) for the data and the fits (dashed lines).

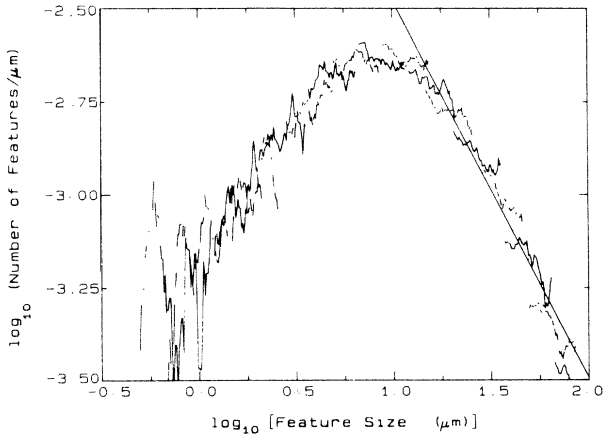

FIG. 5. Log-log plot of the number of features per micrometer versus the feature size for novaculite. The peak in the curve indicates that the sample is not a fractal. The slope of the solid line is -1.

gram for all the feature sizes in the image. In addition to the distribution of features within the image, Eq. (6) is able to model the change in the histograms with magnification. Figure 3 demonstrates the differences between the measured histograms and the fits for a high and low magnification. Also shown in Fig. 3 are the cumulative feature distributions $F(L)$ defined by Eq. (4). The excellent match of the equations and the data demonstrates that Eq. (6) is adequate to describe the feature counting.

B. Log-log plots

A rough way to determine if the number of features per unit length versus the feature size is a power law is to make a log-log plot of the histograms, and then to fit a straight line to the results as described previously. The results are shown in Fig. 4, in which the data for alternate magnifications are dashed. The measurements for neighboring magnifications overlap. The data represent a histogram of counts, so the curves are intrinsically rough; smoother curves may be made by combining neighboring points. A linear least-squares fit provides starting values for the parameters in Eq. (6). Results for a sandstone which does not show a power-law distribution of features are shown in Fig. 5.

C. Fitting to obtain a fractal dimension

Results for a simultaneous fit to a range of magnifications are shown in Fig. 6. The proper modeling of the scaling of the cumulative feature distributions with magnification is a sensitive indicator of a power-law feature distribution.

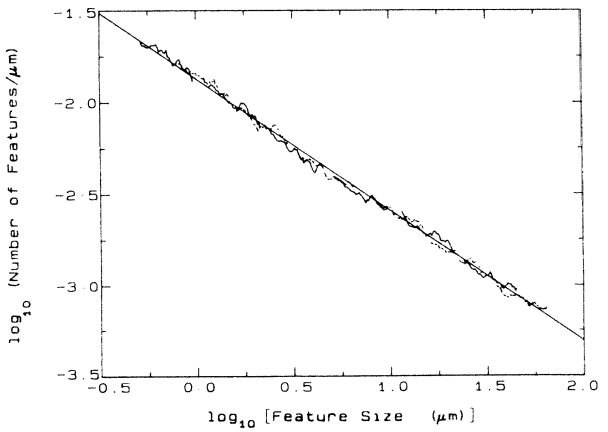

FIG. 4. Log-log plot of the number of features per micrometer versus the feature size for all feature sizes measured at each magnification. Data from alternate magnifications are dashed. Solid line is a linear least-squares fit to the data.

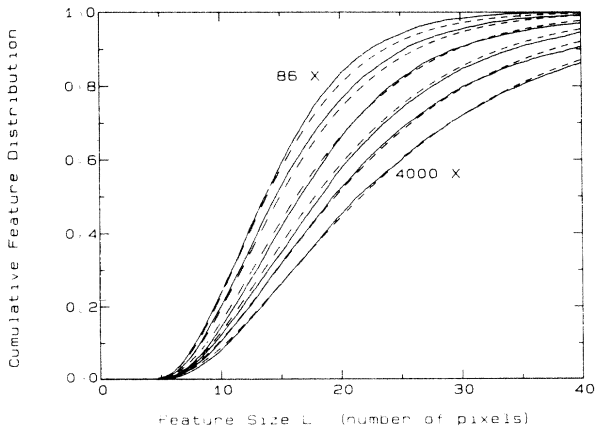

FIG. 6. Cumulative feature distributions for data from different magnifications and the resulting fit (dashed lines) for these magnifications. The cumulative feature distributions show scaling from high to low magnifications starting from 4000× and extending to 86×. Every other magnification in the fit has been displayed.

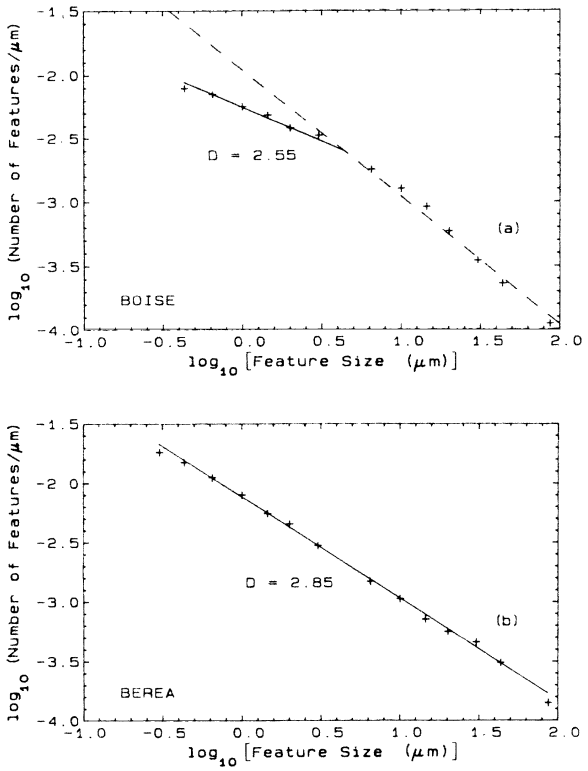

FIG. 7. Results comparing two sandstones with extreme values of the fractal dimension. Plus signs represent fits to individual magnifications, solid lines are the result of simultaneous fits to a range of magnifications, and dashed lines are lines with slope of -1.0 which match data beyond the fractal regime.

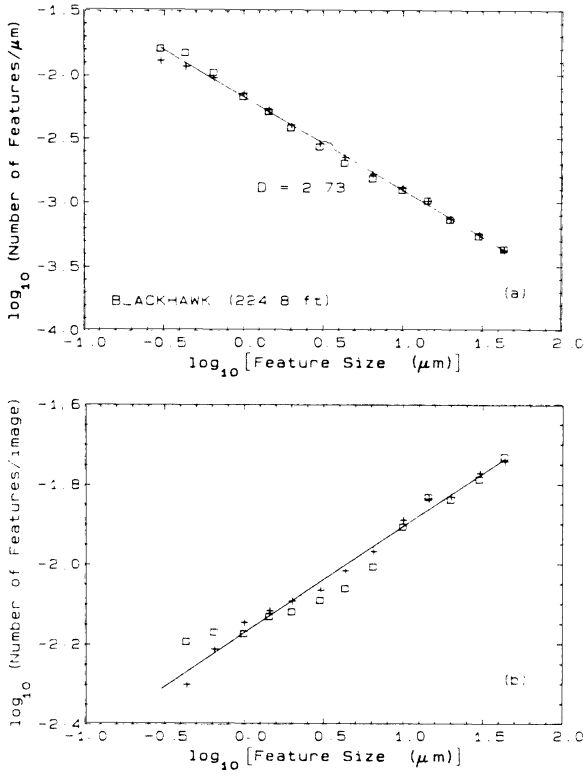

FIG. 8. Results for a Blackhawk sandstone showing behavior for a single position (squares) and for the average of four positions (plus signs). (a) Log-log plot of the number of features per micrometer with a slope of $2-D$. (b) Log-log plot of the number of features per image with a slope of $3-D$.

Results for five sandstones are shown in Figs. 7–10. The individual points represent the fits to the individual magnifications. The solid lines are the results of fitting the feature distributions for a range of magnifications and are generated from the parameters A and D. The fractal dimensions range from 2.55 to 2.85. The dashed lines represent lines of slope -1 which are fitted to the lower magnifications. This is the expected behavior for magnifications beyond the fractal regime where the data looks like statistically random noise. In this homogeneous regime, the individual cumulative feature distributions no longer scale as in Fig. 6, but they overlap.

The absolute values for the number of features per micrometer and for the parameters A and D agree for all the methods of analyzing the data discussed above. For example, the log-log plots of the feature histograms such as in Fig. 4 overlap the plots made by fitting individual magnifications as in Fig. 8. In addition, the parameters A and D determined by fitting Eq. (6) to the data are the same parameters as the slope and the y intercept determined by a linear least-squares fit to the log-log plots, as in Figs. 4 and 8.

IV. DISCUSSION

In this section, the technique will be evaluated. In particular, the effect of including more positions and making

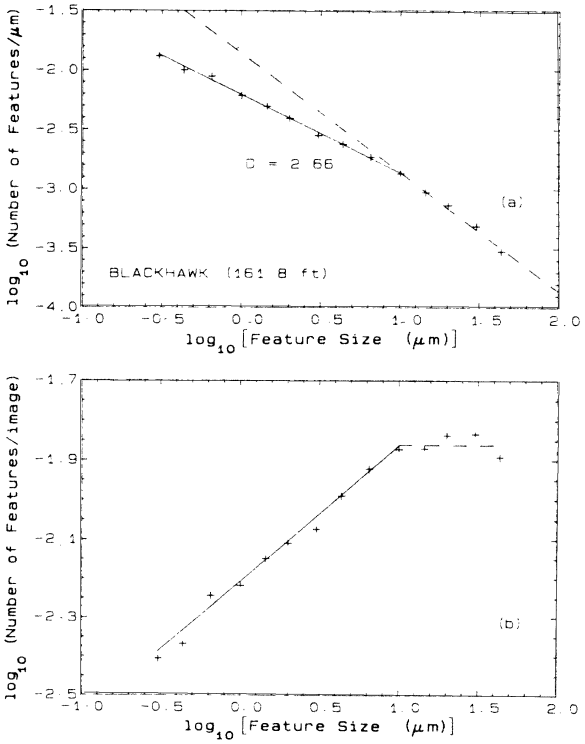

FIG. 9. Results for a Blackhawk sandstone showing the transition to nonfractal behavior at the long-length limit.

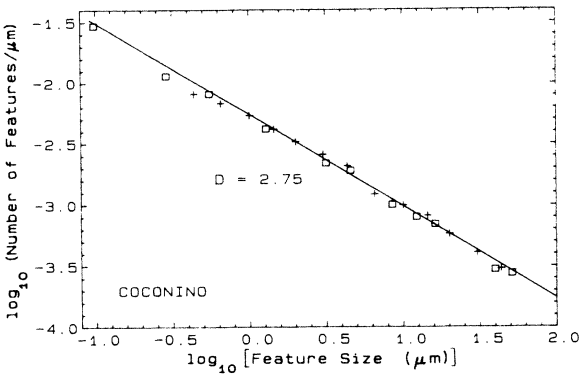

FIG. 10. Results from Coconino sandstone comparing results of the automatic technique (plus signs and solid line) to the results of the manual counting of features (squares).

changes in the technique, such as using a different filter frequency, noise threshold, etc., will be discussed.

A. Comparison of different samples

A dozen sandstones, a chalk, and a shale have been found to be fractal from the highest magnification which could be examined to some lower magnification. The measured fractal dimensions ranged from 2.55 to 2.85, as shown in Figs. 7—10. The samples include standard outcrop rocks such as Boise, Berea, and Coconino as well as sandstones from the Blackhawk formation from a well near Price River, Utah. There is a large range in porosity and permeability of the samples as shown in Table I. The long-length limit l_2, which represents the end of the fractal range, can be seen as a transition from a slope that is less than -1.0 to one which is equal to -1.0. In general, smaller values of the long-length limit correlate with lower values of the fractal dimension. As can be seen in Table I, neither the fractal dimension nor the long-length limit is related to the averaged grain size of the sandstones.

Log-log plots of the number of features counted per micrometer are not sensitive to the scatter in the data because the data are scaled by the field of view at each magnification. Figures 8(a) and 9(a) are replotted as the logarithm of the number of features counted per image. In this case, the points can be fit to a slope of $3-D$, and points beyond the fractal regime are fit to a line with slope of zero. The transition from the fractal regime to the nonfractal regime is more striking on a plot like Fig. 9(b) than a plot like Fig. 9(a).

Only one sandstone, a novaculite, was found not to have fractal behavior. The novaculite or Arkansas stone is an unusual, clean sandstone composed of uniform microcrystalline quartz which appears to be thermally metamorphosed.[6] Arkansas stone is commonly used as a whetstone. The peak in the number of features in Fig. 5 correspond to the size of the microcrystals, and the decrease in the number of small features is explained by the total lack of clays and fine structure in this rock. At lengths larger than the peak, the curve has a slope of -1.0 corresponding to the homogeneous regime. Similar behavior with a narrower distribution was measured for a slide of 1-μm latex spheres. We consider the novaculite to be an atypical example of sandstone behavior.

B. Comparison to a manual technique

Figure 10 compares data analyzed by the automatic technique and data for the same sample analyzed manually. The fractal dimensions measured with the two methods agree within the statistical uncertainty of the data. The manual results were reported by Katz and Thompson.[1] The measurement was made by placing a scale on SEM photographs. Using the full discrimination

TABLE I. Properties of samples used in the fractal measurements.

Sample	Porosity (%)	Permeability (mD)	Grain size (μm)	Fractal D	L_2[a] (μm)
Berea	20	123	190	2.85	>32
Boise (Table)	35	4933	330	2.55	5
Coconino	9.9	0.037	120	2.75	>50
Navajo	18	246	210	2.74	>50
St. Peter's	9.3	5.15	140	2.61	18
Blackhawk sandstones from well near Price River, Utah.					
137.3 ft	12	1.8	120	2.60	18
154.8 ft	4.3	0.02	100	2.59	20
161.7 ft	11.5	21.7	180	2.66	11
169.3 ft	14.3	13.6	200	2.72	22
224.8 ft	7.5	0.02	70	2.73	>50
Austin chalk				2.59	6.3
Carboniforous shale	17			2.74	>10

[a]Limits L_2 marked with the $>$ symbol were not seen with the SEM data. The SEM data then set a lower bound for L_2.

of the eye, a count was made of the number of scale units which were occupied by edges. To compare the two techniques, the manually acquired data were offset by a constant to match the automatic data; the offset is consistent with the higher number of counts found for the larger unit (histogram bin) size used by the manual technique.

C. Comparison to autocorrelation measurements

The results plotted in Fig. 8 were compared to autocorrelation measurements by Katz and Thompson in Fig. 2 of their paper.[1] The autocorrelation measurements were made on a thin section of an epoxy-impregnated sample. The data from the SEM measurements of a fracture surface match the autocorrelation function for the smaller length scales. In addition, their estimate of a long-length limit to the fractal regime of about 65 μm is in agreement with the fact that no limit was measured by the SEM technique for this sample, an indication that the limit was larger than 50 μm.

D. Effect of varying the position

The results for a single position on a sample are shown in Fig. 8 along with an average of four positions. The averaged data show less variance from the fitted line than the data for the single position. The values of the fractal dimension obtained do not change appreciably. The fractal dimensions for the individual positions were 2.73, 2.70, 2.74, and 2.73. The averaged value was 2.73. The first position with $D=2.73$ represents a best choice of locations based on the criteria given in Sec. II.

Sometimes the results from a single position are not enough to determine whether the rock is a fractal, either because a poor location has been chosen or because that particular sample requires measurement of a larger area to obtain good statistics. The resulting cumulative feature distributions do not scale in a proper way to get a good fit as shown by the residues. In these cases, averaging several positions was found to produce acceptable data. The estimated precision for measuring the fractal dimension for the sample in Fig. 8 with four averages is ± 0.01. For only one position, it can be as good as ± 0.02 for a good set of data, as shown in Fig. 9.

E. Effect of noise and filtering

If noise is counted as features, the effect is to greatly increase the number of features counted at the higher magnifications while only slightly increasing the number of features counted at the lower magnifications. The result of counting noise is to increase the measured fractal dimension. (White noise has a slope of -1.0 on the log-log plots.) To confirm that noise was not a problem, we made measurements with two different scan speeds of the SEM; more noise is seen at the faster rates. The two measurements gave the same fractal dimension; this indicates that the amplitude threshold is adequate to prevent erroneous results.

The measured results are insensitive to changes in the resolution for detecting features, changing either the filter or the noise threshold. If the resolution is drastically lowered, fewer features are counted: The statistics are poor and the results are not as dependable.

F. Effects of losing microscope resolution

The smallest feature size which can be measured with this technique is limited by the JEOL 35C SEM. At magnifications above 4000×, there is a decrease in the relative resolution of the image. These images do not appear as sharp as lower magnifications, and the resulting feature histogram shows a lack of features detected at the smaller feature sizes. At magnifications higher than 4000× the capabilities of the SEM rather than the digital filter determine the resolution. This decrease in resolution is so substantial that merely changing the digital filter is not enough to extend the measurement to smaller lengths.

Several additional problems are found at high magnifications. Since fewer features are counted, the statistics are not as good. Also, it is possible to find bigger discrepancies between images from different positions. Finally, features at higher magnifications have poor signal-to-noise because of the decreasing feature amplitudes found at the high magnifications. Features are small because they are frequently found on top of light underlying objects. To get the best data requires care in selecting the positions. If possible, extra positions at the higher magnifications should be included.

V. CONCLUSIONS

A body of data has been collected which confirms fractal behavior for the feature distribution measured along the pore-rock interface of sandstones. These measurements allow the determination of the fractal dimension with a high precision of ± 0.01. In addition to the fractal dimension, the long-length limit for the fractal regime was defined and measured on some samples. Beyond the long-length limit in the homogeneous regime, the data on a log-log plot could be fitted with a slope of -1; this indicates that the geometrical features appear as statistically random noise. A short-length limit for the fractal regime could not be determined by these measurements; it is less than 0.2 μm, the smallest feature size which could be examined.

Most sandstones measured demonstrated fractal behavior over some length range. The one exception is novaculite which has a feature distribution dominated by the size of its microcrystalline-quartz grains. The fractal dimensions ranged from 2.55 to 2.85. The long-length limit to the fractal regime was directly correlated with the fractal dimension and uncorrelated with the grain size. The lack of correlation with grain size implies that diagenesis and not depositional processes determines the fractal properties.

Confidence in the fractal behavior is given by the success of the model feature distribution in describing the statistics for all of the feature sizes in each image. In particular, the model accounts correctly for the scaling with magnification, which is a sensitive indicator of a power-law distribution of features. Variance of the data from the fitted curves is reduced with the addition of more po-

sitions in the analysis demonstrating that the variance arises from statistical fluctuations. Tests for errors in the technique showed that the results are not dependent on such factors as noise and filtering. In addition, the results of the automatic technique agree well with other techniques.

ACKNOWLEDGMENTS

We would like to thank D. H. Johnston for the use of his data on outcrop rocks included in Table I. Also, we would like to acknowledge many helpful discussions with A. J. Katz, and the assistance of R. W. Brown with the SEM and geological interpretations.

[1]A. J. Katz and A. H. Thompson, Phys. Rev. Lett. **54**, 1325 (1985).

[2]B. B. Mandelbrot, *The Fractal Geometry of Nature* (Freeman, San Francisco, 1982).

[3]J. Serra, *Image Analysis and Mathematical Morphology* (Academic, London, 1982), pp. 152–158.

[4]G. Nagy, Computer **16**, 13 (1983).

[5]R. H. Pennington, *Introductory Computer Methods and Numerical Analysis,* 2nd ed. (Macmillan, Toronto, 1970), pp. 417–421.

[6]W. D. Keller, G. W. Viele, and C. H. Johnson, J. Sediment. Petro. **47**, 834 (1977).